Co-electrodeposition of iron and sulfur in aqueous and non-aqueous electrolytes

V.A Majidzade[1*], S. P. Mammadova[1], E. S. Petkucheva, E. P. Slavcheva[2], A. Sh. Aliyev[1], D. B. Tagiyev[1]

[1]*Acad. M.Nagiyev Institute of Catalysis and lnorganic Chemistry NAS of Azerbaijan, AZ 1143, H.Javid ave. 113, Baku, Azerbaijan*
[2]*Acad. Evgeni Budevsk Institute of Electrochemistry and Energy Systems - Bulgarian Academy of Sciences, Akad. G. Bonchev 10, 1113 Sofia, Bulgaria*

The work is devoted to the electrochemical co-deposition of iron and sulfur on Pt substrates from aqueous and nonaqueous electrolytes. The potential range of the single Fe and S and the bi-component Fe-S thin film electrodeposition is determined by applying the potentiodynamic polarization curves. The mechanism of the proceeding faradaic reactions on the surface of the platinum substrate is studied and identified in a broad potential range. The structure, stoichiometry, and morphology of Fe-S thin films deposited by potentiostatic and galvanostatic methods are determined using SEM, EDXA and X-ray phase analysis. The comparison of the results obtained in aqueous and non-aqueous electrolyte showed that Fe-S electrodeposition on the platinum substrate occurs by a similar mechanism in aqueous and non-aqueous electrolytes within a relatively broad potential range as in aqueous media, the process is facilitated due to the higher electrical conductivity of the electrolyte.

Keywords: Fe-S films, electrodeposition, semiconductors

INTRODUCTION

The demand for obtaining two-component or multicomponent semiconductor materials is related both to the development of solar energy, based on the use of thin layers of semiconductor materials and the various practical applications of semiconductor chalcogenides in micro- and optoelectronics [1-9]. Such materials are used to create miniature amplifiers and generators of electrical signals operating in a wide frequency range; integrated circuits for modern computers; converters of one type energy to another one [10-14]; thin-layered solar cells for energy production and storage [15-16]; semiconductor light emitting diodes; lasers and photo-detectors operating within infrared and visible light ranges; components of the fiber optic cables for communication; radiation and particle detectors; magnetic, piezoelectric, ferroelectric and many other devices.

The thin FeS_2 (pirite) films are known for their valuable properties for photoelectric and photoelectrochemical applications [17]. They are also considered as potential solar absorber material due to several factors among which the main is the suitable gap between their energy zones (0.95 eV) with a high optical absorption coefficient ($\alpha \approx 5 \times 10^5$ cm^{-1}) and a sufficiently long minority carrier diffusion length to produce short circuit currents >30 mA. Thanks to the high absorption coefficient, even a very thin FeS_2 film can capture the great part of the reflecting solar radiation, as the theoretical conversion efficiency is about 20%. In addition, FeS_2 has demonstrated catalytic ability [18]. Finally, Fe and S are extremely widespread, cheap, and non-toxic materials [19].

Various methods are used to obtain thin pyrite films among which gas-phase methods such as sputtering and organometallic chemical vapor deposition [20, 21]; phase-solution methods such as spray pyrolysis, chemical bath deposition [17, 22], electrophoretic deposition, sol-gel [20] and sulfurization of electrochemically deposited Fe-S layers [23-26]. The hydrothermal method is the most attractive synthesis and processing method because it enables ideal control of morphology, purity, crystallinity, composition and low cost for large-scale production [27-29]. The hydrothermal treatment is also testified with respect to annealing, in order to increase efficiency and improve the optoelectronic properties of electrodeposited semiconductor materials [28].

In comparison with the above mention methods, the electrochemical deposition of FeS_2 is relatively simple and very economical [30–31] approach. It does not require expensive equipment and high-temperatures for annealing. The method is very environmentally friendly, has high selectivity, and allows deposition onto complex electrodes of different shapes and large sizes. Electrodeposition in a potentiostatic or galvanostatic mode makes it possible to obtain thin-film semiconductor structures. The goal of this work is to study the mechanism of initial components (Fe and S)

* To whom all correspondence should be sent.
E-mail: vuska_80@mail.ru

electroreduction separately and then to investigate their co- electrodeposition from aqueous and non-aqueous electrolytes, resulting in the formation of thin bi-component Fe-S films.

EXPERIMENTAL

The aqueous and non-aqueous electrolytes used for Fe-S electrodeposition were prepared as Fe- and S- containing salts (0.01 – 0.1 M $Fe(NO_3)_3 \cdot 9H_2O$ and 0.01 – 0.1 M $Na_2S_2O_3 \cdot 5H_2O$) were dissolved separately in bi-distilled water or in ethylene glycol (EG) at a temperature of 313-323 K and then mixed under stirring.

The electrochemical tests were carried out in a three-electrode electrochemical cell with a volume of 100 ml. The working electrode a Pt wire with an area of 0.3 cm^2 onto which the thin Fe, S, and Fe-S films were deposited. As reference and counter electrodes were used silver/silver chloride (Ag/AgCl/KCl) electrode and a Pt sheet with an area of 4 cm^2, respectively. Before electrodeposition, Pt electrodes were pretreated in concentrated nitric acid, washed with bi-distilled water, and kept in boiling nitric acid containing a small amount of ferric chloride for 30 minutes. Next, they were thoroughly washed with distilled water and finally rinsed with alcohol or acetone.

The polarization curves were taken using the "IVIUMSTAT Electrochemical Interface" potentiostat. Firstly, the potentiodynamic polarization method was applied to determine the potential region of the single components electrodeposition. For each test, the potential scan rate was adjusted so that the redox peaks on the voltammogram are clearly distinguished. After that Fe, S, and FeS_x were deposited galvanostaticaly under following conditions: j=22 $mA.cm^{-2}$, t=15 min, bath composition 0.05 M $Fe(NO_3)_3.9H_2O$ + 0.5 $Na_2S_2O_3.5H_2O$ in aqueous media or in ethylene glycol r non aqueous solutions.

The surface structure and morphology of the as prepared films were studied by X-ray diffraction (XRD). The diffraction data were collected using X-ray diffractometer PhilipsADP15 with Cu-Kα(λ–1.54178 Ǎ) radiation at a constant rate of 0.20 $s^{\square 1}$ over an angle range 2Ө-10-900.

The crystal structure and phase identification of the catalytic films were examined by scanning electron microscopy (SEM) with a JEM-200CX, JEOL (80 keV accelerating voltage and magnification up to 100,000) microscope.

RESULTS AND DISCUSSION

Figure 1 shows the polarization curve recorded in aqueous electrolyte, containing: 0.1M $Fe(NO_3)_3 \cdot 9H_2O$. As can be seen, there are two well-

shaped current peaks on the curve, related to electroreduction of iron ions on the substrate surface. The first peak formed in the potential range from 0.68 to -0.36 V is due to reduction of Fe (III) to Fe (II) (eq.1), while the second peak situated at potentials from -0.36- to -0.8 V can be prescribed to further reduction of Fe (II) to atomic iron in a two-electron reaction (eq. 2) [32].

$$Fe^{3+} + e^- = Fe^{2+} \qquad (1)$$

$$Fe^{2+} + 2e^- = Fe^0 \qquad (2)$$
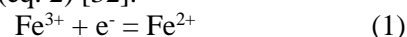
At potential values more negative than -0.8 V, metallic iron is deposited on the substrate.
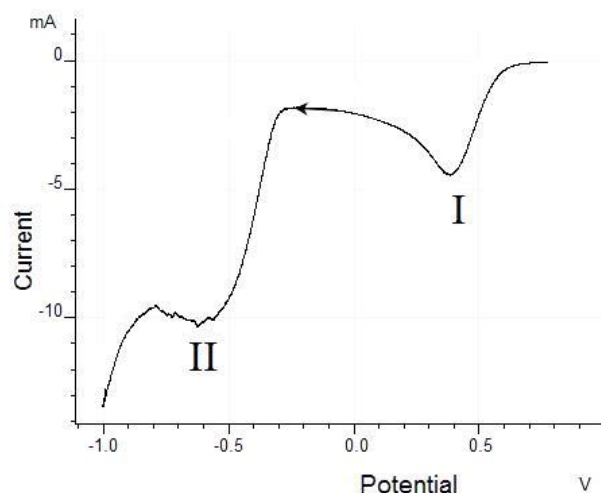
Fig. 1. Potentiodynamic polarization curve presenting the electroreduction of Fe^{3+} ions on Pt electrode in 0.1M Fe $(NO_3)_3$ aqueous electrolyte; scan rate 0.04 $(V.s^{-1})$; temperature 293 K

The electroreduction process of thiosulfate ions from an aqueous 0.1M $Na_2S_2O_3$ electrolyte is shown in Figure 2. It can be seen that this reaction occurs in the potential range from -0.3 to -0.9 V in one stage according to eq. (3):

$$S_2O_3^{2-} + 6H^+ + 8e = 2S^{2-} + 3H_2O \qquad (3)$$

After determining the range of potentials where the electrochemical reduction of individual components occurs, the co-electrodeposition of iron and sulfur from mixed 0.1 M $Fe(NO_3)_3$ + 0.1M $Na_2S_2O_3$ aqueous electrolyte was studied. Figure 3 shows the obtained cyclic potentiodynamic curve. As it is seen, several cathodic and anodic peaks are observed in the course of the process.
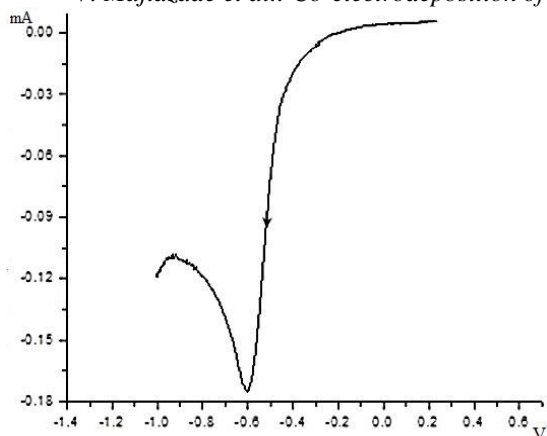
Fig.2. Potentiodynamic polarization curve presenting the electroreduction of thiosulfate ions on Pt electrode from aqueous 0.1M $Na_2S_2O_3$ electrolyte; scan rate 0.02 $V.s^{-1}$; temperature 293 K

On the cathode part of the curve, within the potential interval from 0.65 V to -0.63 V, reduction peaks (I and II) of thiosulfate to sulfide ions is observed. The reaction proceeds according the eq. (4):

$$S_2O_3^{2-} + 6H^+ + 8e \rightarrow 2S^{2-} + 3H_2O \qquad (4)$$
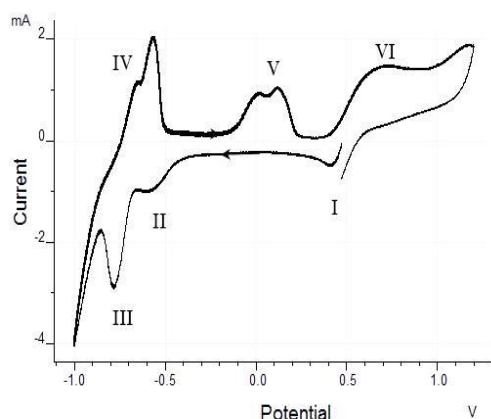
Fig. 3. Potentiodynamic cyclic polarization curve of co-electro deposition of Fe and S on Pt electrode from 0.1 M $Fe(NO_3)_3$ + 0.1M $Na_2S_2O_3$ aqueous electrolyte; scan rate 0.08 $V.s^{-1}$; temperature 293 K

In the following section of the cathodic polarization curve (from -0.7 to -0.9 V), co-deposition of Fe-S occurs (peak III) according to the eq. (5):

$$2Fe^{+3} + 4S^{2-} + 2H^+ \rightarrow 2FeS_2 + H_2 \qquad (5)$$
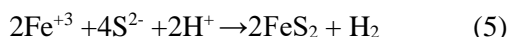
Then, at potentials more negative than -0.87 V trivalent iron is reduced and deposited on the surface in atomic state.

On the anode branch of the cyclic polarization curve, first the processes of dissolution of iron to Fe^{2+} and Fe^{3+} ions (peak IV) occurs, then the deposited FeS_2 dissolves to Fe^{3+} and S^{2-} ions (peak
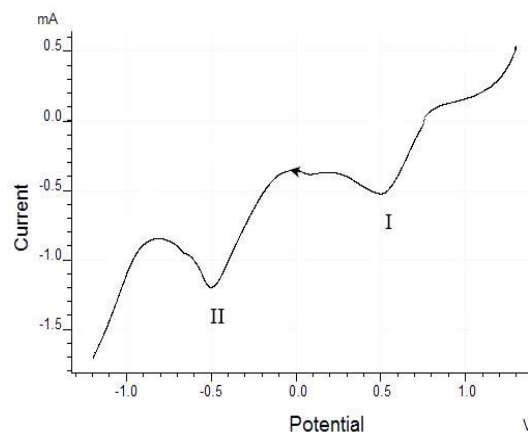
Fig. 4. Potentiodynamic polarization curve presenting the electroreduction of Fe^{3+} ions on Pt electrode in nonaqueous 0.1M $Fe(NO_3)_3$ + CH_2OH-CH_2OH electrolyte; scan rate 0.02 V, temperature 293 K

V). The last peak VI corresponds to dissolution of S^{2-} to elemental S^o.

For comparison, the same experiments were carried out using non-aqueous ethylene glycol solutions. Figure 4 shows the polarization curve of the process of electroreduction of Fe^{3+} ions on Pt electrode from EG solution of 0.1M $Fe(NO_3)_3$.
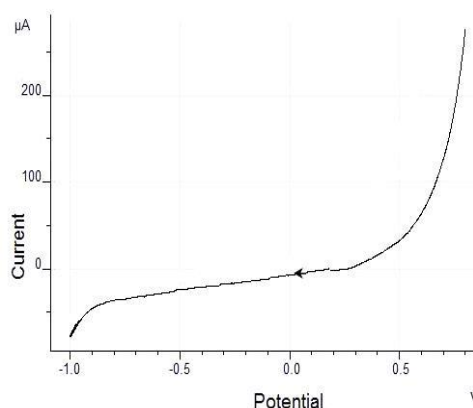
Fig. 5. Potentiodynamic polarization curve presenting the electroreduction of thiosulfate ions on Pt electrode in 0,1 M $Na_2S_2O_3$ nonaqueous EG electrolyte; scan rate 0.02 V/s; temperature 293 K

The comparison of Figure 1 and Figure 4, shows that the electroreduction of Fe^{3+} ions in an aqueous and nonaqueous media occurs by the same mechanism with slight differences in the rate of the surface reactions due to the difference in electrical conductivity of both electrolytes.

In the case of thiosulfate ions, the electroreduction also occurs in a single stage, but at more negative potentials. The comparison of Figure 2 and Figure 5 shows that in aqueous media, the process begins at the potential value of -0.3 V, while in non-aqueous media this occurs at much more negative potentials (-0.9 V).
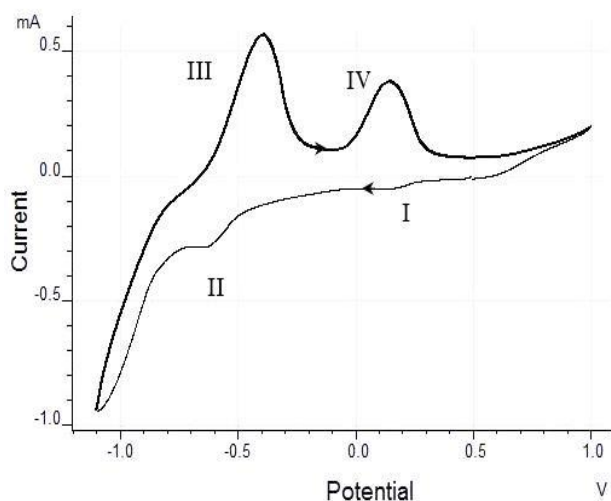
Fig. 6. Potentiodynamic cyclic polarization curve presenting the co-electrodeposition of Fe and S on Pt electrode from a mixed 0.1M $Fe(NO_3)_3$ + 0.1M $Na_2S_2O_3$ non-aqueous (EG) electrolyte; scan rate 0.03 V/s, temperature 293 K

Figure 6 shows the electrochemical co-deposition of Fe and S from an ethylene glycol solution. On the cathode part of the curve, two current peaks are distinguished. The first peak (I) appears in the potential range from 0.60 to 0.35 V and is related to reduction of Fe^{3+} to Fe^{2+} ions. Further reduction of iron is observed in the potential range from -0.45 to -0.73 V (peak II), whiles the process of Fe-S co-deposition starts at around -0.9 V and intensifies at more negative potentials. The assumed reaction mechanism at the reverse potential scan includes the dissolution of the obtained Fe-S film in the potential range from -0.65 to -0.3 V, (peak III), while at potentials from -0.1 to 0.25 V (peak IV), thiosulfate ions dissolve with the formation of various ions.
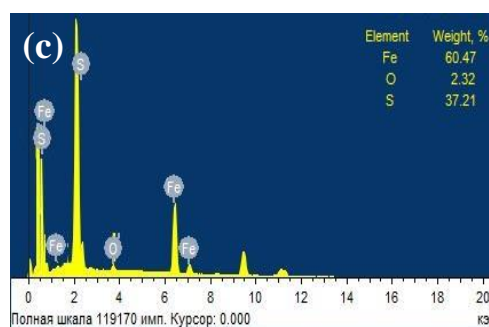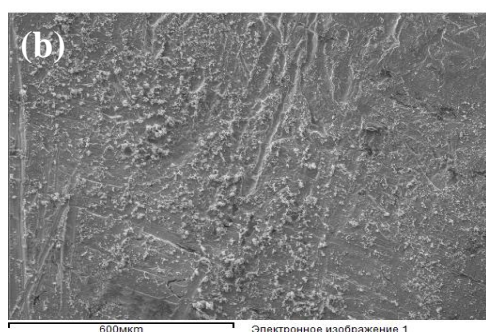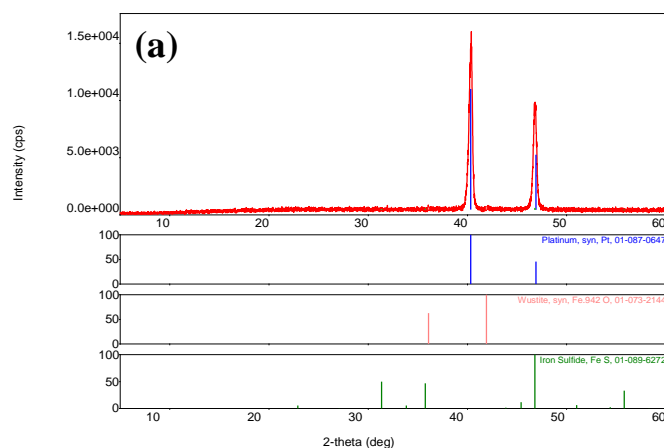
Fig. 7. XRD pattern (a), EDAX (b) and SEM (c) image of thin Fe-S films on a Pt electrode from aqueous electrolyte

The obtained samples were studied using SEM and X-ray phase analysis. The data obtained are shown in Figures 7 and 8. The results prove the co-electrodeposition of Fe and S on the Pt for both studied samples. The XRD patterns of the samples obtained from aqueous and non-aqueous electrolytes consist of two phases, which conform to Fe-S and iron oxides.

The EDAX analysis also shows the spectra of iron, sulfur, and oxygen. In samples obtained from a non-aqueous electrolyte, oxygen spectra are not seen. Therefore, it can be assumed that the films obtained from ethylene glycol solution are of higher quality, since the composition of these films is closer to the stoichiometric composition of FeS and they have better adhesion to the electrode surface.

76
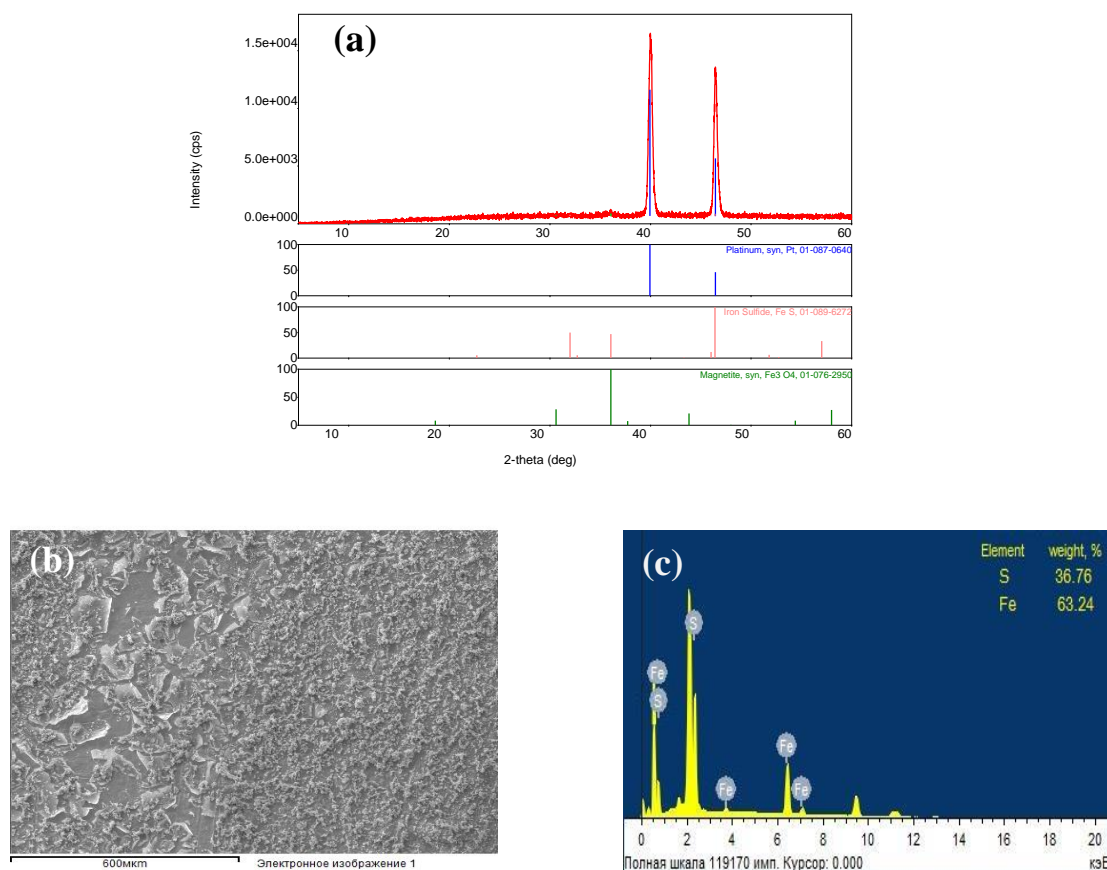
Fig. 8. XRD pattern (a), EDAX (b) and SEM (c) image of thin Fe-S films on a Pt electrode from non-aqueous (EG) electrolyte

CONCLUSIONS

The research performed demonstrated that the electrochemical co-deposition is an easy and efficient approach to obtain bi-component semiconductor materials. It was found that the Fe-S electrodeposition on the platinum substrate from aqueous and non-aqueous ethylene glycol electrolytes occurs by a similar mechanism of the proceeding surface reactions within a relatively broad potential range. The Fe-S co-deposition in aqueous electrolyte starts at about -0.4 V, while in EG the reaction is shifted to much negative potential of about - 0.9 V. Thus, it can be concluded that in aqueous media, the process is facilitated due to the higher electrical conductivity of the electrolyte. Further research is currently in progress to investigate how the type of electrolyte affects the mechanical and corrosion stability, as well to evaluate photosensitive and electrocatalytic properties of the electrodeposited Fe-S films.

REFERENCES

1. P. Tonndorf, R. Schmidt, P. Böttger, X.. Zhang, J. Borner, et al. *Opt. Express*, **21**, 4908 (2013).
2. G. M.Huseynov, N. A. Mammadova, H. A. Imanov, *Chem. Problems* , **15** , 329 (2017).
3. W. He, H. Zhang, Y. Zhang, M. Liu, X. Zhang, F. Yang, *J. Nanomater.* (2015)
4. V.A., Majidzade, *Chem.l Problems*., **16**, 331 (2018).
5. A. Sh. Aliyev, V. A. Majidzade, N. Sh. Soltanova, D. B. Tagiyev, V. N. Fateev, *Chem.Problems.*, **16**, 178 (2018).
6. D. S. Sofronov, E. A. Vaksler, Y. A. Bondarenko, V.V. Starikov et. al., *Inorg. Mater*., **52**, 1205 (2016).

7. C. Agapescu, A. Cojocaru, A. Cotarta, T. Visan. *J. Appl. Electrochem.,* **43**, 309 (2013).
8. V. A. Majidzade, S. F. Cafarova, A. Sh. Aliyev, D. B. Tagiyev, *Azərb. Kimya J.*, **3**, 6 (2018).
9. E.A., *Streltsov Bulletin of BSU.*, Ser. **2**., 1 (2011).

10. Ch. Li, F. Wang, Y. Chen, L. Wu, J. Zhang, et. al., *Mater. Sci. Semicond. Process.,* **83**, 89 (2018).

11. W. Liyanage, J. Wilson, Ed. Kinzel, B. Durant, Nath. Manashi, *Sol. Energy Mater. Sol. Cells,* **133**, 260 (2015).

12. D. Boosagulla, Sr. Mandati, R. Allikayala, B. V. Sarada, *ECS J. Solid State Sci. Technol*., **7**, 440.

13. Ch. Chen, D. C. Bobela, Y. Yang, Sh. Lu, et. al. *Front. Optoelectron.,* **10**, 18 (2017).

14. S. Im, C.S. Lim, J. Chang, Y. Lee, N. Maiti et. al., *Nano Lett.*, **11**, 4789 (2011).

15. V. N. Fateev, O. K. Alexeeva, S. V. Korobtsev E. A. Seregina, et. al., *Chem. Problems,* **16**, 4, 453 (2018).

16. T. L. Kulova, I. I. Nikolaev, V. N. Fateev, A. Sh. Aliyev, *Chem. Problems*., **16**, 9 (2018).

17. V. Aluri, K. T. Reddy, Y. M. Reddy, *Nanotechnol. Rev.* , **4**, 469 (2015).

18. Jasion D. Thesis , 2015

19. Sh. Kawai, R. Yamazaki, S. Sobue, E., Okuno, M. Ichimura, *APL Materials*, **2**, 032110 (2014) .

20. S. Seefeld, M., Limpinsel, Y. Liu, N. Farhi, et. al. *J. Am. Chem. Soc*., **135**, 4412 (2013).

21. S. Kment, H. Kmentova, A. Sarkar, R. J. Soukup, et.al. *J. Alloys Compd*., **607**, 169 (2014).

22. K. Anuar, W. T. Tan, N. Saravanan, S. M. Ho, S. Y. Gwee, *Pac. J. Sci. Technol*., **10**, 801 (2009).

23. X. Wang, G. Wang, J. Chen, X. Zhu, et. al., *Mater. Lett.,* **110**, 144 (2013).

24. A. Gomes, J. R. Ares, I. J. Ferrer, M. I. S. Pereira, C. Sanchez, *Mater. Res. Bull*., **38**, 1123 (2003).

25. Y. Z. Dong, Y. F. Zheng, H. Duan, Y. F. Sun, Y. H. Chen, *Mater. Lett.,* **59**, 2398 (2005).

26. Y. Z. Dong, Y. F. Zheng, X. G. Zhang, H. Duan, et. al., *Sci. China Ser. E*, **48**, 601 (2005).

27. S. Nakamura, A. Yamamoto, *Sol. Energy Mater.Sol. Cells*, **65**, 79 (2001).

28. N. Yu, L. Du, H. Du, Z. Mao, et. al. *Thin Solid Films*, **550**, 206 (2014).

29. R. Henríquez, C. Vasquez, N. Briones, E. Muñoz, P. Leyton, E. A. Dalchiele, *Int. J. Electrochem. Sci*., **11**, 4966 (2016) .

30. P. Prabukanthan, R. Lakshmi, T. R. Kumar, S. Thamaraiselvi, G. Harichandran, *Adv. Mater. Proceedings,* **2**, 521 (2017).

31. M. Ichimura, T. Kajima, Sh. Kawai, K. Mibu, *Jpn. J. Appl. Phys*., **55**, 038006 (2016).

32. A.A. Sukhotin (Ed): Handbook of Electrochemistry, Chemistry, Leningrad, Russian, 1981, p.488.